GeoScienceWorld
Lithosphere
Volume 2024, Article ID lithosphere_2023_325, 14 pages
https://doi.org/10.2113/2024/lithosphere_2023_325

Lithosphere

Research Article

Lithospheric Conductivity Structure in the Middle Segment of the Jiangnan Orogenic Belt: Insights into Neoproterozoic Tectonic–Magmatic Processes

Jiayong Yan,[1,2] Hui Chen,[1,2,3] Juzhi Deng,[2,3] Hui Yu,[2,3] Yuexin You,[2,3] Yidan Wen,[2,3] and Min Feng[2,3]

[1]*SinoProbe laboratory of Chinese Academy of Geological Sciences, Beijing, 100094, China*
[2]*State Key Laboratory of Nuclear Resources and Environment, East China University of Technology, Nanchang, 330013, China*
[3]*School of Geophysics and Measurement-control Technology, East China University of Technology, Nanchang, 330013, China*

Correspondence should be addressed to Hui Chen; huich@ecut.edu.cn

Received 31 October 2023; Accepted 6 February 2024; Published 1 March 2024

Academic Editor: Jiyuan Yin

The Jiangnan Orogenic Belt (JOB) evolved from the Yangtze and Cathaysia blocks through multi-stage oceanic-continental subduction, collisional orogeny, and intracontinental deformation, which is an important region to study the formation and evolution of the South China Continent (SCC). Magnetotelluric soundings were collected along a 520-km-long northwest (NW)-trending profile across the middle segment of the JOB to explore the possible remnants of ancient tectonic–magmatic processes beneath the central SCC by combining with the satellite gravity and magnetic data. The resistivity model reveals that the crust in the middle segment of the JOB and its adjacent area is characterized by high resistivity anomalies, while the uppermost mantle is characterized as medium resistivity anomalies and separated by several subvertical, lithospheric-scale conductors. Two trans-crust anomalies of high conductivity and low density beneath the Jiujiang–Shitai Buried fault (JSBF) and Jiangshan–Shaoxing fault (JSF) extend south-eastward to the lithosphere, which are attributed to the NW and southeast boundaries of the middle segment of the JOB. The imaged NW-trending of JSF reflects the tectonic process of the JOB subducting under the Cathaysia Block. Two lower-crustal conductors also imaged beneath the Jiuling area are interpreted as the partial melting of the lower crust, which may be related to the deep southeast subduction of the Paleo-south China Ocean during 970 to 860 Ma. In addition, the trans-lithosphere high conductivity adjacent to the ancient collisional zone of the Jinning period II (ACZII) is probably related to the asthenosphere upwelling caused by the soft collision between the Yangtze and Cathaysia Blocks, which triggered the contemporaneous magmatism in the Jiuling area. This work provides a new insight into the lithospheric evolution in SCC during the Neoproterozoic.

1. Introduction

The South China Continent (SCC) is located at the junction of the Paleo-Asian Ocean, Tethys, and Pacific tectonic domains, bordered by the North China Block to the north, the Indochina Block to the south, the Qinghai-Tibet Plateau to the west, and the West-Pacific Plate to the east [1] . Its present status comes from the composite evolution of multi-stage plate tectonics in the Paleo-south China Block, making it one of the most complex geological evolution history areas since the Neoproterozoic [2, 3]. The Jiangnan Orogenic Belt (JOB) in the middle of SCC is spread in a NE-NEE direction, with the Yangtze Block on the northwest (NW) and the Cathaysia Block on the southeast (Figure 1). This area records the collisional assembly of these two ancient microplates, which is of great significance for understanding the crustal accretion, tectonic evolution in the SCC, and the breakup of supercontinent Rodinia [4, 5].

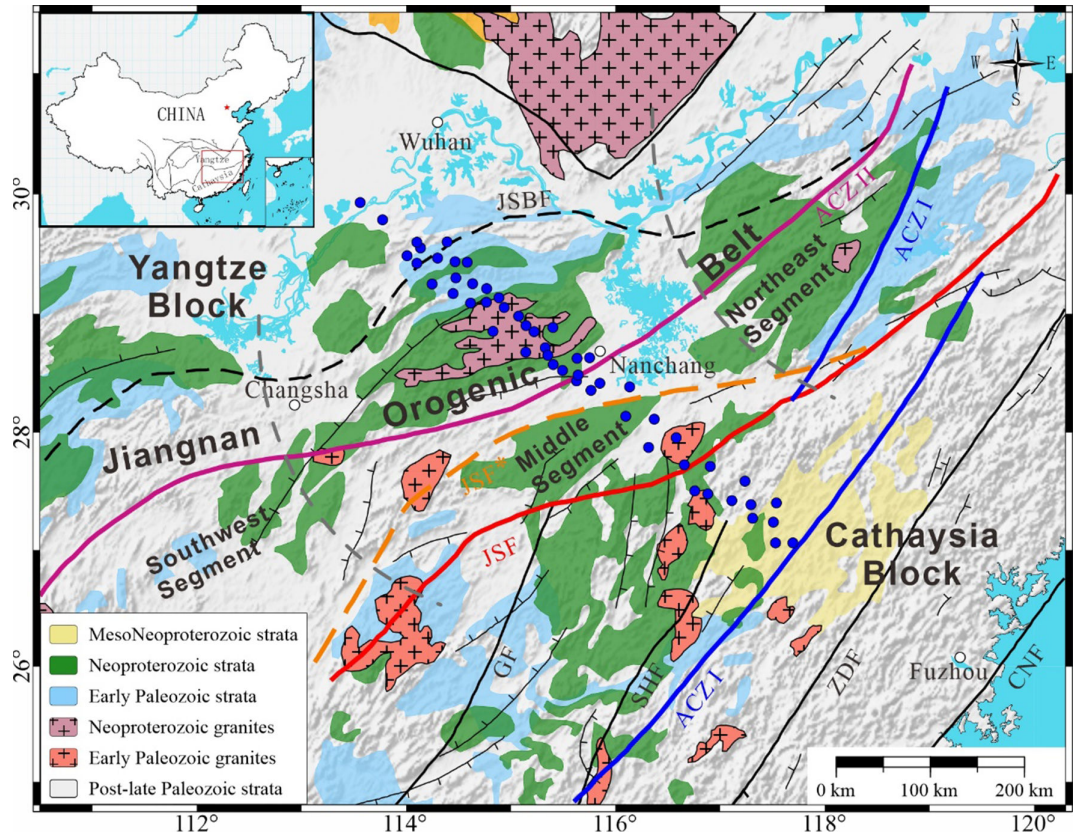

FIGURE 1: The location of magnetotelluric (MT) stations and geological sketch map of the study area [2, 38]. ACZ I, Ancient collisional zone of the Jinning period I; ACZ II, Ancient collisional zone of the Jinning period II; CNF, Changle-Nanao Fault; GF, Ganjiang Faults; JSBF, Jiujiang–Shitai buried fault; JSF/JSF*, Jiangshan–Shaoxing fault; Middle Segment, Jiuling terrane; Northeast Segment, Huaiyu or Shuangxiwu terrane; SHF, Shaowu-Heyuan Fault; Southwest Segment, northern Hunan Province and northern Guangxi Province terrane; ZDF, Zhenghe–Dapu Fault.

Previously proposed models for the tectonic evolution of the JOB include (1) plate subduction collision model [6, 7]; (2) plume model [8]; and (3) plate-rift model [9]. The first model suggests that there is a "trench-arc-basin" system related to ocean crust subduction in the JOB [6], and its magmatic action occurs in 1.0–0.75 Ga, with three stages of the orogenic process consisting of oceanic crust subduction, continental collision, and post-orogenic extension [7]. The second model advances the subduction collision of the Yangtze and Cathaysia Blocks to 1.3–0.8 Ga in the late Middle Proterozoic, points out that the JOB is part of Greenwell orogeny, and attributes the granite formed during the Neoproterozoic period of 850–750 Ma to the crust remelting triggered by mantle plume activity [8]. The third model is a relatively compromise view, which suggests that the edge of the Yangtze Block underwent extensive subduction during the late Meso-Proterozoic period from 1.3 to 0.96 Ga, followed by arc-continent collision during the Neoproterozoic period from 960 to 860 Ma, which remelted the newly formed crust. The JOB was formed by the collision between the Yangtze and Cathaysia Blocks that occurred during 830 to 800 Ma, which caused the crustal thickening and structural collapse [9]. In addition, the formation of the JOB is also believed to be caused by the divergent double subduction of the Paleo-south China Ocean towards the Yangtze and Cathaysia Blocks based on the characteristics of the early Neoproterozoic volcanic arc assemblage found on both sides of this area [10].

The existing debates are at least partly due to the poorly-resolved lithospheric structure of SCC that records the assembly of Yangtze Block and Cathaysia Block and the boundaries of the JOB that hampers understanding of the lithospheric evolution in SCC during the Neoproterozoic. Previous geological and geophysical research works have actively promoted the understanding and recognition of deep tectonic and dynamic processes in the SCC [5, 11–13]. However, the absence of exposed magmatic rock due to the thick sedimentary cover in the middle segment of the JOB prevents insights into the tectonic–magmatic processes occurring beneath the study area. Therefore, geophysical imaging of the subsurface structure beneath the JOB is key to understanding the tectonic–magmatic processes in the SCC.

The magnetotelluric (MT) has been widely used in the study of lithospheric structure due to its advantages of large detection depth and high efficiency [14–20]. However, for the SCC, previously reported MT observations either focused on the entire SCC or are largely restricted to western part of SCC [12, 13]. In this study, we present results from an MT survey along a north-west profile

crossing the middle segment of the JOB. We employed a three-dimensional (3-D) inversion approach to determine the electrical structure of the lithosphere and examined the possible origins of the major resolved electrical features and their tectonic implications. By combining regional, geological, and geophysical data, we intend to give new insight into the tectonic boundary and its deep extension beneath the middle segment of the JOB and the deep process between the Yangtze and Cathaysia blocks. This work may shed new light on our understanding of the formation and evolution of the JOB.

2. Geological and Geophysical Settings

The JOB spreads out at the junction of the Yangtze and Cathaysia blocks, extending from northern Guangxi Province in the west, passing through Guizhou Province, western Hunan Province, Jiangxi Province, southern Anhui Province, and western Zhejiang Province to northern Zhejiang Province, it extends for over 1500 km, and is about 200 km wide (Figure 1). The JOB can be roughly divided into three parts: the northeast segment (Huaiyu or Shuangxiwu terrane), the middle segment (Jiuling terrane), and the southwest segment (northern Hunan Province and northern Guangxi Province terrane), mainly composed of Meso-Neoproterozoic low-grade metamorphic strata, Neoproterozoic granite, a small amount of mafic rocks, and two widely recognized sets of Serpentine belt [4, 11]. Among them, the outcrop strata are mainly composed of Nanhua volcanic sedimentary rocks, giant thick rift sedimentary rocks of the Nanhua system that have not undergone metamorphism or low-grade metamorphism, and stable shallow sea sedimentary sequences from the Sinian to Early Palaeozoic. The folded basement includes Shuangxiwu Group, Xikou Group, Shuangqiao Mountain Group, Sipu Group, Lengjiaxi Group, and Banxi Group, which are mainly composed of a set of greenschist facies metamorphic schist and argillaceous rock, sandwiched felsic tuff, spilite, and base-ultrabasic rocks [21–23]. The age of Neoproterozoic magmatic rocks here is mainly concentrated at 950 to 750 Ma, forming a significant peak around 820 Ma. Its lithology is mainly aluminous granite and a small amount of siliceous basalt, mafic–ultramafic rock, forming the Bendong, Sanfang, Yuanbaoshan intrusions in the southwest segment, the Jiuling intrusions in the middle segment, and the Xucun, Shexian, and Xiuning intrusions in the northeast segment. Among them, the Jiuling intrusions in the middle segment of the JOB mainly intruded into the Shuangqiaoshan Group [22, 24, 25].

The existing tectonic pattern of the JOB is mainly controlled by a series of tectonic movements since the Middle and Late Jurassic periods, including the development of regional deep faults and their dissection into uplift and depression blocks [23]. The main faults in the area include the Jiujiang–Shitai Buried Fault (JSBF) and the Anhua–Luocheng fault, which are distributed in a nearly NE direction in the NW, the NEE direction Yifeng–Jingdezhen fault located in the central part and the nearly NE direction Jiangshan–Shaoxing fault (JSF) located in the southeast [3, 23, 26]. The tectonic deformation of the JOB mainly includes the reversed S-shaped structure system formed by the collision of Yangtze and Cathaysia blocks in the Jinning period, the complex tectonic system formed by the closure of the South China rift system in the Caledonian, and the composite tectonic system formed by intracontinental orogeny in the Indochina–Yanshanian period [11]. At present, the academic community has a comprehensive understanding of the boundary location, diagenetic environment, and regional tectonic evolution of the northeastern segment of the JOB [2, 4], but the degree of research on the middle and southern segments is relatively weak, especially the tectonic boundary location, deep boundary extension and lithospheric subduction process of the middle segment are still controversial [11, 13].

In recent years, a large number of deep exploration studies have been carried out in the SCC using geophysical methods and achieved fruitful results. Based on the two-dimensional (2-D) inversion results of the MT profile across Jingdezhen and Wenzhou, Han et al. [27] concluded that the Cathaysia Block squeezed into the Yangtze Block near the upper mantle of the northeastern segment of the JOB, pointing out that the JSF is the southeast boundary of the JOB in this segment. Xu et al. [12] believed that the JSF is tilted southeast in the deep part of the Wuyishan region based on the results of the 3-D inversion of MT covering Southeast of the SCC, and pointed out that the tectonic pattern is the result of the combined effect of late Cretaceous shear stretching and rift valley movement. Zhang et al. [28] further revealed the deep contact relationship and deep processes of the Yangtze and the Cathaysia blocks by using the 2-D inversion results of three MT profiles passing through the northeast, middle, and southwest segments of the JOB. Mao et al. [13] deduced that the Kaiyuan–Pingtang and Pingxiang–Chaling faults are the western and eastern boundaries of the orogenic belt through the 2-D inversion of MT profiles across the southern segment of the JOB. Dong et al. [29] based on the 2-D and 3-D inversion results of two MT profiles passing through the northeast and middle segment of the JOB, suggested that the Yangtze Block has crossed the JOB in the deep part and squeezed into the Cathaysia plot near the JSF. Yan et al. [5] combined geophysical and geochemical data to further demarcate the north–south tectonic boundary of the JOB. Although the above research results have a positive role in improving the understanding of the deep structure and formation process of the SCC, relatively few studies on the deep structure of the middle segment of the JOB.

3. Magnetotelluric Method and Data

3.1 Data Acquisition and Processing. The MT data came from the geological survey project of China Geological Survey undertaken by the Chinese Academy of Geological Sciences, with a total of 52 sites, and was collected along an NW-trending profile crossing the middle segment of the JOB. This profile starts near Honghu Lake in the Jianghan Basin, crossing the Mufushan Uplift, Xiuwu Basin, Jiuling

Uplift, Pingle Depression, and Ganhang Tectonic Belt, and ends near Shaowu in the Wuyi Uplift, with a total length of about 520 km (Figure 1). The MT method measures two horizontal magnetic field components (Hx and Hy), one vertical magnetic field component (Hz), and two horizontal electric field components (Ex and Ey). Data were acquired from 52 sites, using a Phoenix MTU-5A electromagnetic sounding system (Phoenix Geophysics Ltd, Canada). The recording time was >20 hours for each site, and time series were processed via a discrete Fourier transform method with a robust algorithm [30] and a remote reference technique to solve for the MT transfer functions using the bundled SSMT2000 software provided by Phoenix Ltd (Canada). The impedance data were computed in the frequency range of 320–0.001Hz, and the data quality was analyzed by the data error and continuity of the apparent resistivity and impedance phase curves. We introduced an auto-selection method that deletes data that are strongly influenced by noise and stores high-quality data.

Figure 2 shows the apparent resistivity and impedance phase curves of six typical MT sites in the study area, among which, the MT sites shown in Figure 2(a) and (b) are located near the JSBF on the NW side of the JOB, from which it can be found that the apparent resistivity amplitude of these MT sites first increases and then decreases with the decrease of frequency, and is generally lower than 100 Ω m, reflecting the overall low resistivity in this area. The MT sites shown in Figure 2(c), (d) and (e), are located within the JOB. The apparent resistivity and components of each measuring station in the figure are curved apart in the period range greater than 1 second, and the *xy* and *yx* components of the apparent resistivity are high, indicating that there is obvious structural inhomogeneity in the shallow and deep parts of the JOB, and there may be high resistance anomalies in the middle and lower crust. The measuring stations shown in Figure 2(f) are located in the Wuyi uplift zone of the Cathaysia block. The apparent resistivity of the measurement point also shows a trend of increasing first and then decreasing with frequency, but the apparent resistivity amplitude at the highest frequency is greater than 1000 Ω m and the resistivity amplitude at the lowest frequency is still greater than 100 Ω m, indicating that the Wuyi uplift belt has higher resistivity distribution characteristics than that of Yangtze and JOB.

3.2 Phase Tensor Analysis. The analysis of dimensional and electrical strike of MT data is the premise for determining the dimensional characteristics and the strike direction of the regional conductivity structure, and then reasonably selecting inversion methods [31]. Traditional MT data analysis methods such as Swift de-composition, Bahr decomposition, and G-B decomposition may be affected by galvanic distortion may lead to deviation in the analysis results, while the phase tensor method does not require 2-D assumptions and is not affected by galvanic distortion caused by superficial local anomalies [31], and has been widely used in MT data analysis [32]. Therefore, the phase tensor method is used to analyze the acquired MT data, and the phase tensor minimum and 2-D deviation distribution of each measuring station on the profile are obtained.

Figure 3(a) shows the distribution of phase tensor minimum (Φ_{min}) for all MT sites, which reflects the trend of underground resistivity. High Φ_{min} reflects a decrease in resistivity, corresponding to the red ellipse in the figure, while low Φ_{min} reflects an increase in resistivity, corresponding to the blue ellipse in the figure. Therefore, the gradient process of ellipse color from red to blue in the figure indicates that the underground changes from a low-resistance zone to a high-resistance zone. From the difference of Φ_{min} with the frequency of each measuring station in the figure (the direction of the section arrow in the figure is south–east, and the blank space without filling the ellipse indicates the disturbed frequency point data that is rejected), the high-frequency Φ_{min} is lower and the low-frequency Φ_{min} is higher in the range between the Jiuling uplift in the NW segment and the Wuyi uplift in the southeast segment of the profile, indicating that the shallow resistivity in this area is higher and the deep resistivity is gradually decreasing. The low-frequency Φ_{min} in the Yangtze Block and the Pingle depression of the JOB is small, reflecting the high resistance characteristics of its depth. Figure 3(b) shows the 2-D deviation (β) distribution of all MT sites, and the change of this parameter with frequency reflects the dimensional characteristics of different depths of the underground sphere. It is generally believed that the absolute value of the β is less than 3 and stable over a frequency range, indicating that the subsurface medium is a non-3-D structure, and vice versa, indicating that the subsurface medium has 3-D properties [31, 32]. In addition, the major and minor axes of the phase tensor ellipse are determined by the rotational invariants Φ_{max} and Φ_{min}, respectively, so their shape can also indicate the dimensional characteristics of underground structures. When the shape of an ellipse in a certain area is approximately circular, it indicates that the area is close to a one-dimensional (1-D) structure, and when the shape of the ellipse is approximately "needle-like," it indicates that the subsurface medium tends to a 3-D structure. As shown in Figure 3, most of the MT sites are less than 3° in the β of the middle- and high-frequency bands, and the high-frequency β of a small number of MT sites is greater than 3°, reflecting that the shallow layer is dominated by 2-D structures and there are local 3-D structures. With the decrease in frequency, most of the MT sites β greater than 3°, and the number of "needle-like" ellipses gradually increased, indicating that the deep part of the study area was dominated by 3-D structures. Therefore, the MT 3-D inversion method used in this study can provide a reliable electrical structure model.

4. Three-Dimensional Inversion and Results

4.1 Three-Dimensional Inversion. The 3-D inversions of the profile data were performed using the ModEM code based on the Nonlinear Conjugate Gradient algorithm [33]. In order to improve the efficiency of the inversion, the selected data were resampled to 30 frequencies in the effective frequency range of 320–0.001 Hz. The off-diagonal

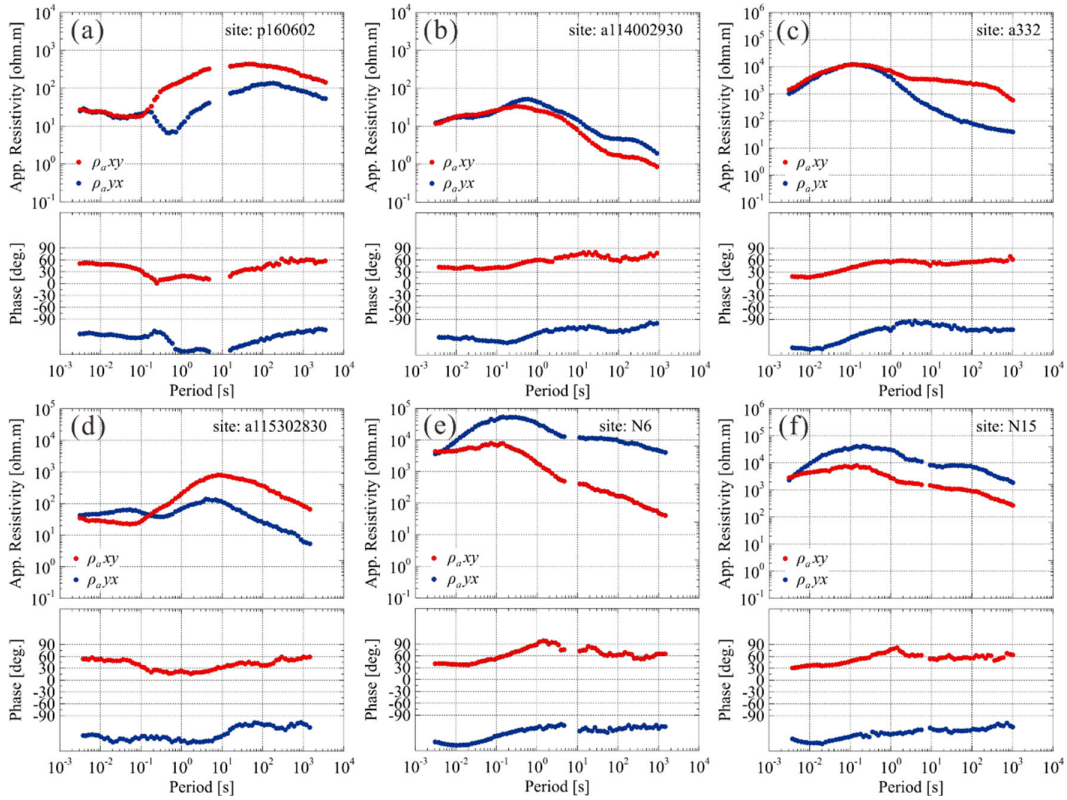

FIGURE 2: Typical apparent resistivity and impedance phase curves of MT sounding

impedances were used, and the error floor was set to 5%*|Zxy*Zyx|$^{(1/2)}$, so as to ensure the stability of the inversion. According to the distribution range and average spacing of MT sites, the inversion model was discretized using a horizontal grid with 88 × 67 grid nodes at 5 km spacing in the core, surrounded by 12 layers of nodes with the size increasing exponentially outward by a multiplier of 1.3. We divided the model vertically into 48 layers, starting with a thickness of 50 m and increasing geometrically with a multiplier of 1.2. Hence, the starting model was a homogeneous background discretized by 112 × 91 × 48 cells with a resistivity of 100 Ω m. In addition, the model covariance was set to 0.2, the initial regularization factor λ_0 was set to 1000, the cooling factor ρ was set to 10, and the target regularization factor λ_{min} was set to 10^{-6}. After 179 iterations, an acceptable nRMS misfit of 2.49 was achieved. The comparison of apparent resistivity and impedance phase between individual measured data and inversion model response is shown in Figure 4. In general, the modeled responses can fit the data and the differences between the two are small.

4.2 Sensitivity Tests. In order to verify the reliability of the inversion results, we perform the sensitivity tests by replacing the value of the typical high-conductivity anomaly in the preferred model with the background resistivity. Forward modeling was then performed. The test schemes include replacing the resistivity of C1, C2, C3, C4, and C5 with a resistivity of 100 Ω m, and replacing deep parts of the preferred model with 100 Ω m below 60 km. The modified model and the comparison between the responses and the original observations are shown in Figure 5. It can be found that after changing the resistivity of C1, C2, C3, C4, and C5, the nRMS values of the corresponding MT sites all change greatly, indicating that the model response after replacing these high-conductivity anomalies will be difficult to fit the field observation data. It cannot truly reflect the electrical distribution characteristics of the subsurface and also verify the authenticity and reliability of these high conductivities. Although the nRMS value of most MT sites also changes greatly after changing the resistivity of the high-conductivity anomaly below 60 km in the entire profile, the nRMS change amount of some MT sites in the range of 215–280 km is almost 0, indicating that the preferred model is not sensitive to the electrical distribution below 60 km within the range, which may be related to the insufficient deep constraint of MT data in this area.

4.3 Three-Dimensional Resistivity Model. The electrical distribution of the middle segment of the JOB and adjacent areas at different depths are shown in Figure 6. The four sub-figures in this figure represent the plane top view of depths of 2, 20, 45, and 80 km below sea level, respectively, to reveal the electrical structural characteristics of shallow, crust, and upper mantle. As shown in Figure 6(a), the Yangtze Block exhibits a medium–high resistance anomaly (R2) at a shallow depth, and the range of this anomaly closely matches the Yanshanian granite distribution area located at the northern end of Mufushan. The resistivity value on the NW side of the JOB is less than 100

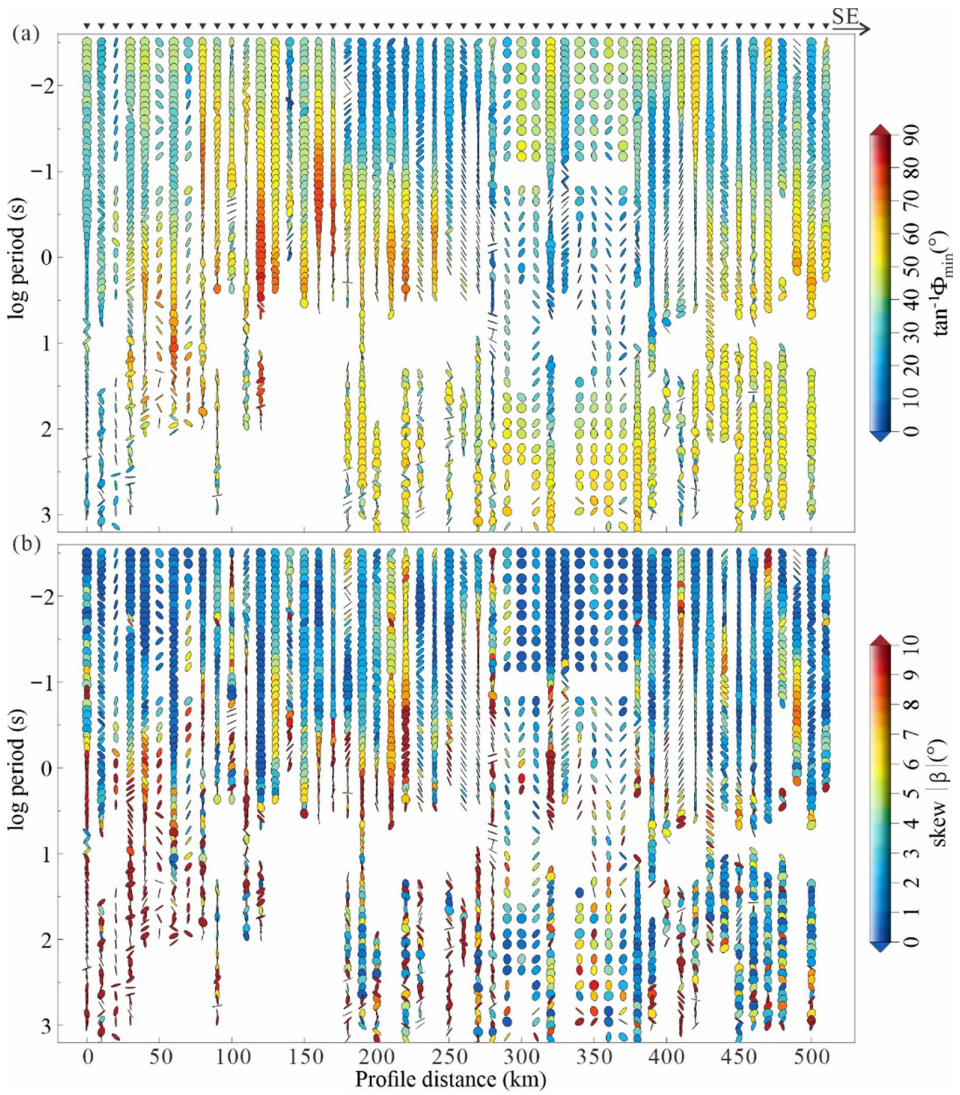

FIGURE 3: Maps of phase-tensor ellipse pseudo-sections for all periods and sites along the profile. Ellipses in Figure 3(a) are colored by the phase tensor minimum (Φ_{min}). Ellipses in Figure 3(b) are colored by skew angle.

Ω m (C2), and its location is just in the coverage area of the Sinian Lower Triassic Strata in the Xiuwu Basin. The resistivity value in the JOB is generally greater than 3000 Ω m, which is basically consistent with the range of Neoproterozoic granite exposed in the Jiuling uplift. The Cathaysia Block shows a widely distributed high-resistance anomaly (R5), which may be an electrical reflection of a shallow large area of granite in the Wuyi uplift. The main manifestation of the shell in the study area is the high-resistance feature (Figure 6(b)), and its resistivity value is generally greater than 1000 Ω m. The high-resistance anomaly R3 in the JOB is likely to be an extension of the shallow Jiuling Neoproterozoic granite in the deep part, which was cut by the high-conductivity anomalies C4 and C5 at this depth. The Cretaceous-Paleogene cap in the Jianghan Basin showed a significant conductivity anomaly (C1). In addition, there is a certain correspondence between the distribution of the deep high-conductivity anomaly and the location of the shallow fault structure, among which C2 has a certain spatial correspondence with JSBF, C5 and ACZII, and C7 and JSF. The resistivity of the mantle in the study area decreased compared with the crust (Figure 6(c)), and at this depth, R2 basically disappeared, and the resistivity of R3, R4, and R5 decreased significantly, and its resistance changed in the range of 300–1000 Ω m. The high-conductivity C2, C4, C5, and C7 in the shell continue to extend upward to the mantle, and there is still a clear mapping relationship with the known fault structure on the surface spatially, and C2 and C7 have a tendency to move downward to the NW. When the depth reaches 80 km (Figure 6(d)), the overall high-conductivity feature of the study area is high, and the abnormal range of C3 and C5 under the Jiuling uplift increases and the resistance decreases significantly.

According to the MT profile electrical distribution and the load ratio and effective elastic thickness, thermal structure, and density derived from the satellite gravity and magnetic data (Figure 7), the lithosphere of the Yangtze Block to the west of the JSBF is dominated by high

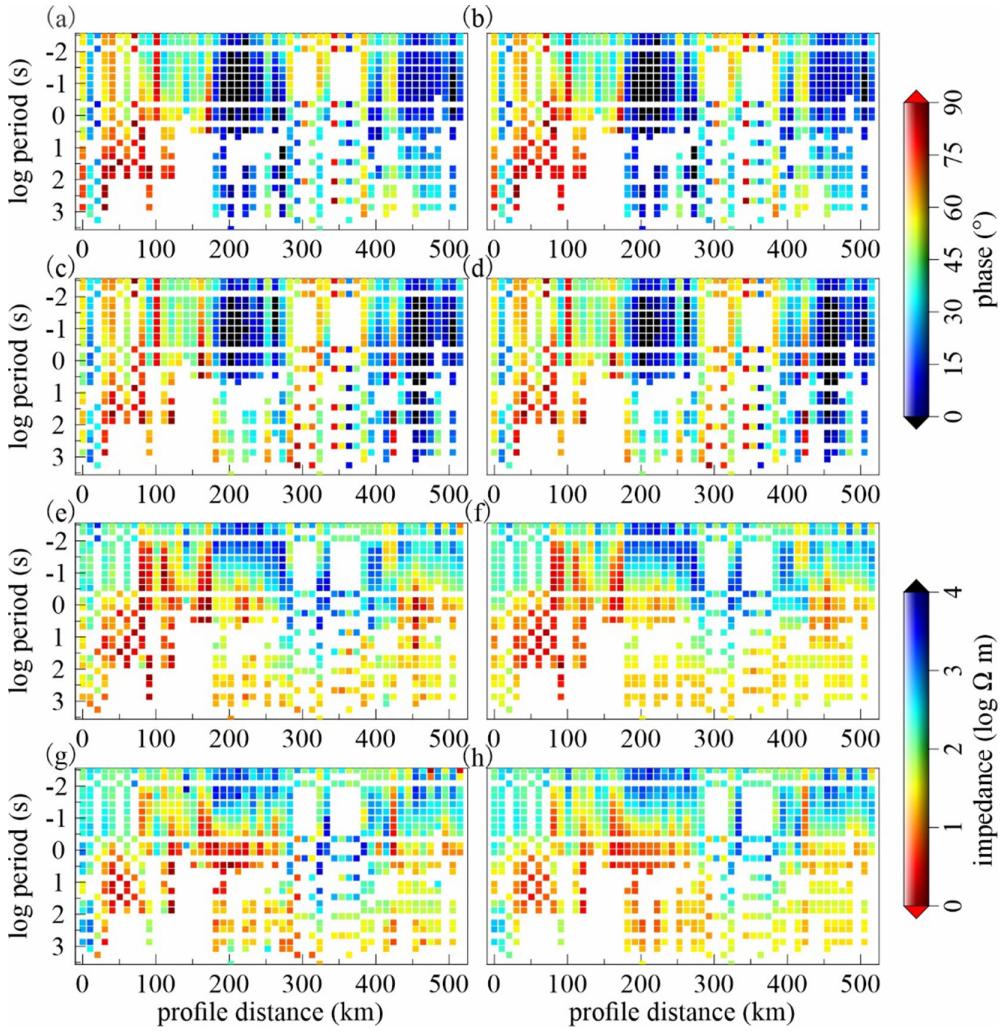

FIGURE 4: Comparison of apparent resistivity and impedance phase between measured data and inversion model response. The sub-figures on the left show the measured apparent resistivity and impedance phase. The sub-figures on the right show the response of the preferred model.

resistivity, and density stratification occurs at about 35 km. The density below this depth is significantly higher than that above. In combination with the Moho discontinuity depth, there is a significant density difference between the crust and upper mantle in this area. Although the crust and upper mantle in this area are dominated by high resistance, the resistance of high resistance (R2) in the crust of the Mufushan area is significantly greater than that of the upper mantle high resistance (R1) under the Jianghan Basin on the NW side, and there is a significant high-conductivity anomaly (C1) in the upper crust of the Jianghan Basin. The reason for this difference in electrical properties and density below the Jianghan Basin may be related to the vertical stratigraphic distribution of the Pre-Sinian metamorphic rock series, Paleozoic–Mesozoic sedimentary rock series, and Cretaceous-Paleogene sedimentary rock series in this area from bottom to top [34]. The high resistance anomaly in the Mufushan area on the southeast side of the Jianghan Basin may be related to the multi-stage composite granite body formed after the Mesozoic continental orogenic [35, 36].

At the location of the JSBF, there is a medium to low resistivity channel that tilts southeast and extends near the Moho surface. Within the Jiuling Uplift on the southeast side, the high resistivity anomaly (R3) extends from the surface to a depth of about 35 km in an inverted triangle shape. There are two high-conductivity anomalies (C4 and C5) in the middle and lower crust depths on the west and east sides of the high resistivity anomaly, respectively, communicating downwards with the upper mantle. The research shows that the main structure in the Xiuwu Basin is the Xiuwu Wuning syncline. The syncline basement is mainly the Metamorphic rock basement of the Shuangqiaoshan Group in the early Neoproterozoic. The main body of the syncline is composed of the Sinian Lower Triassic strata, and the top layer is covered with a small number of Quaternary sediments [37]. The Jiuling uplift developed on the basis of the Jinning Island arc fold belt and is

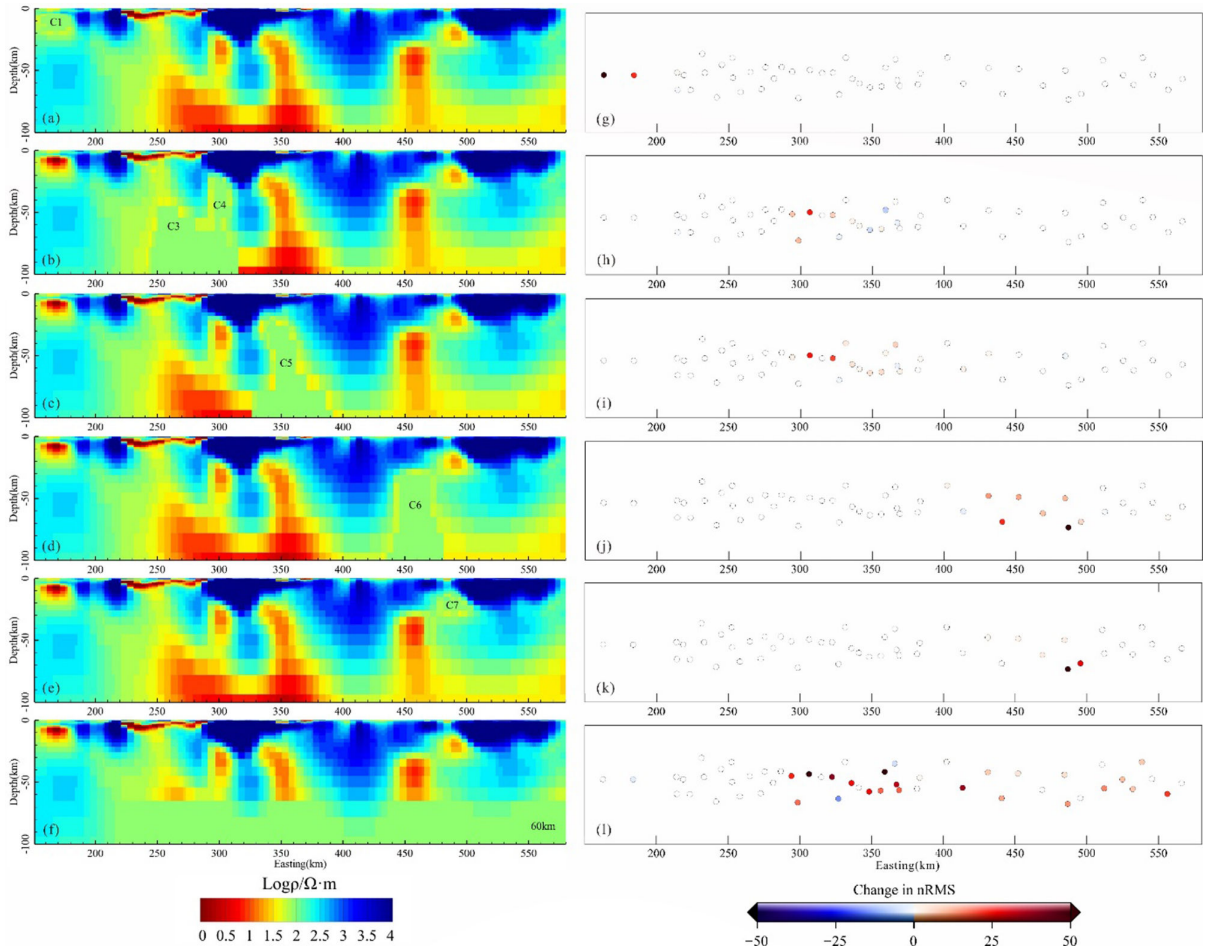

Figure 5: Sensitivity tests for the imaged resistivity features. (a)–(f) The tested models with certain regions replaced by the constant resistivity value of 100 Ω m. (g)–(l) Changes of nRMS in different tests.

mainly composed of Precambrian crystalline basement and Neoproterozoic granites [38–40]. Therefore, the high-resistance anomaly R3 may be a common electrical reflection of the Jiuling Uplift Neoproterozoic granite and the Precambrian crystalline substrate. In addition, the high-conductivity anomaly C2 corresponds well with the Xiuwu Basin, and its high-conductivity characteristics are likely a reflection of the Sinian Lower Triassic strata in the basin. There is a shell mantle-scale electrical gradient zone (C5) under the ACZII, which is on the NW side of the Pingle Depression and tilted to the southeast, with the obvious gravity and magnetic difference between the two sides. The temperature and density of the southeast side are significantly higher than those on the NW side, revealing that the two sides of the high-conductivity anomaly may be two different sets of geological units. The above geophysical phenomena confirm the consensus of previous speculations on the location of ancient plate docking in the region, and are consistent with the geological characteristics of the Wanzai-Yifeng ophiolitic melange belt developed near ACZII [2, 4, 40, 41]. Therefore, C5 is likely to be an extension of ACZII in the deep part, reflecting the soft collision process between the Yangtze Block and the Cathaysia Block. In the Pingle Depression and Ganhang tectonic zone east of ACZII, there is a layered low-resistance anomaly distribution in the shallow part, which may be related to the coal-bearing clastic rocks and sediments developed in the Pingle depression and the shallowly developed red basin strata of the Ganhang tectonic zone [40, 42, 43]. There is a larger range of high-resistance anomaly R4 in its depth, which also extends downward in the shape of an "inverted triangle," but its depth is greater than the extension of R3, reaching about 75 km. Since the Pingle depression belongs to the upper stacked depression basin, it is not integrated on the base of sedimentary metamorphic rocks of the rift valley trough type [40], and the lowest layer of the Ganhang tectonic zone is also a set of metamorphic rock basements [42, 43]. Therefore, it is speculated that R4 is an electrical reflection of the metamorphic rock basement in the region. In addition, there is a near-steep high-conductivity anomaly C6 below the Moho surface of the Ganhang tectonic belt, and a high-conductivity C7 extending southeast to the vicinity of the Moho interface below the JSF on the southeast side.

The crust within the Wuyi Uplift of the Cathaysia Block is primarily distinguished by anomalies of high resistance (R5), and its effective elastic thickness is comparatively small. Both the Moho surface and the interior are relatively

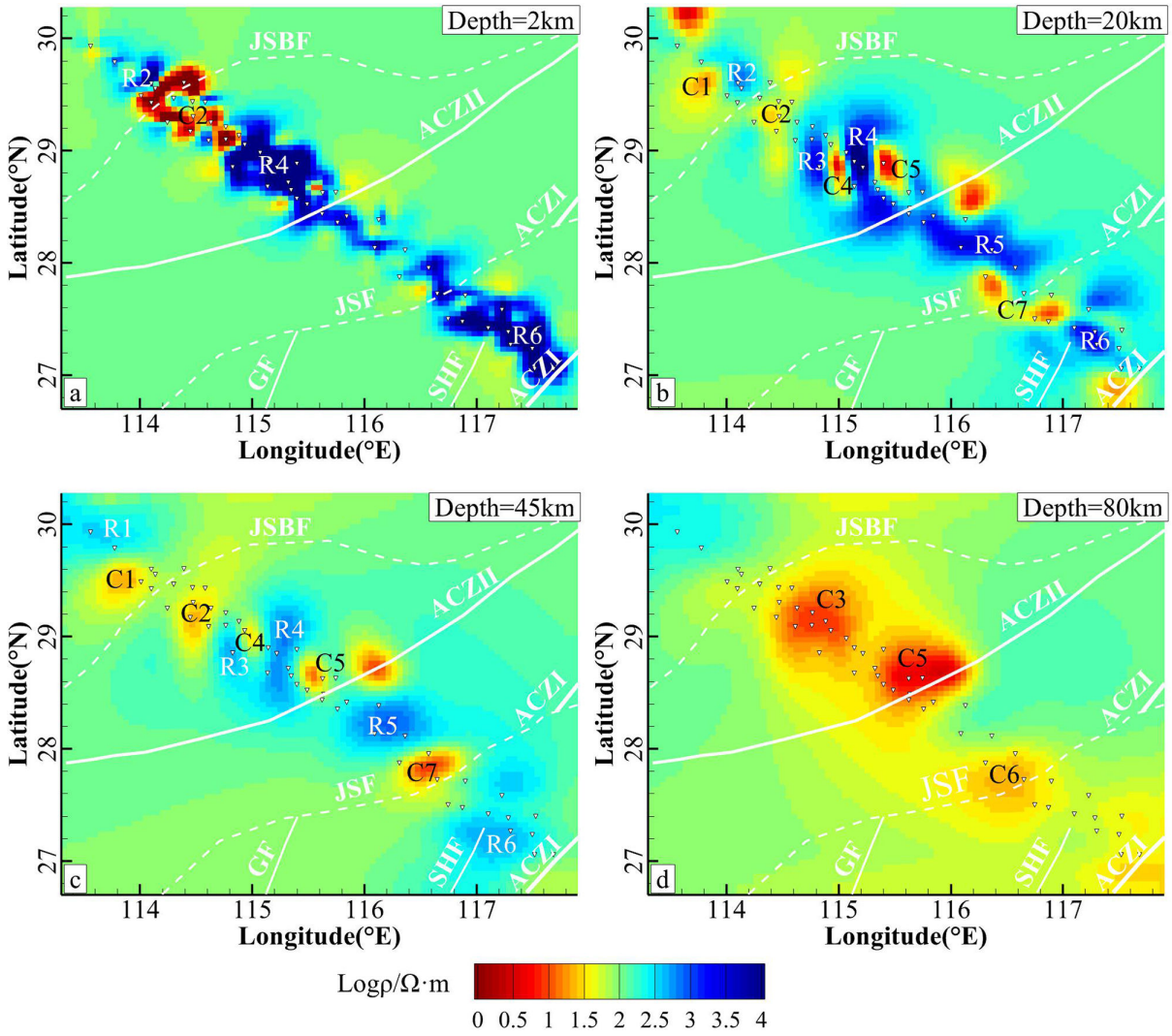

FIGURE 6: Horizontal slices of 3-D inversion model at different depths

shallow. Due to the multiple stages of magmatic activity in the SCC during the late Mesozoic period, widespread volcanic rocks and granular intrusive rocks were formed [4, 38], and deep seismic detection revealed that the Pn wave velocity of the upper mantle in the SCC was high and had a global extension zone structure [44]. Therefore, it is speculated that R5 is the product of late Mesozoic magmatic activity, reflecting the widespread development of volcanic rocks and granites against the background of the stretching of the region.

5. Discussion

5.1 Constraints on the Neoproterozoic Accretionary Boundary

5.1.1 Jiujiang–Shitai Buried Fault. The electrical structure of the middle segment of the JOB revealed in this study is similar to the 2-D electrical structure obtained by predecessors in the southern and middle segments of the JOB [13, 29]. Our results reveal that there are underlying high-conductivity anomalies along the JSBF in the northeast, middle, and west segments of the JOB, which may reflect the extension of the NW boundary of the JOB in deep. At present, the boundary on the NW side of the JOB is less divergent, and most researchers believe that the JSBF is the NW boundary of the JOB [4, 5, 11, 45, 46], but there are different understandings of the extension of the boundary in the deep part and its formation process. According to the geochemical characteristics of the ophiolite melange in the northeast segment of the JOB, predecessors believed that the formation of the early ophiolite might be related to the southeast subduction of the oceanic crust during 970–860 Ma [47]. This is confirmed by the strong imbricate and NW direction thrust nappe structural facies on the NW side discovered by predecessors through deep Reflection seismology in the western segment of the JOB, indicating that there are Neoproterozoic remnants of southeast direction subduction in this area [1]. The characteristics of JSBF inclination in the deep southeast direction revealed in this paper tend to be consistent with the results revealed by previous people, and its spatial

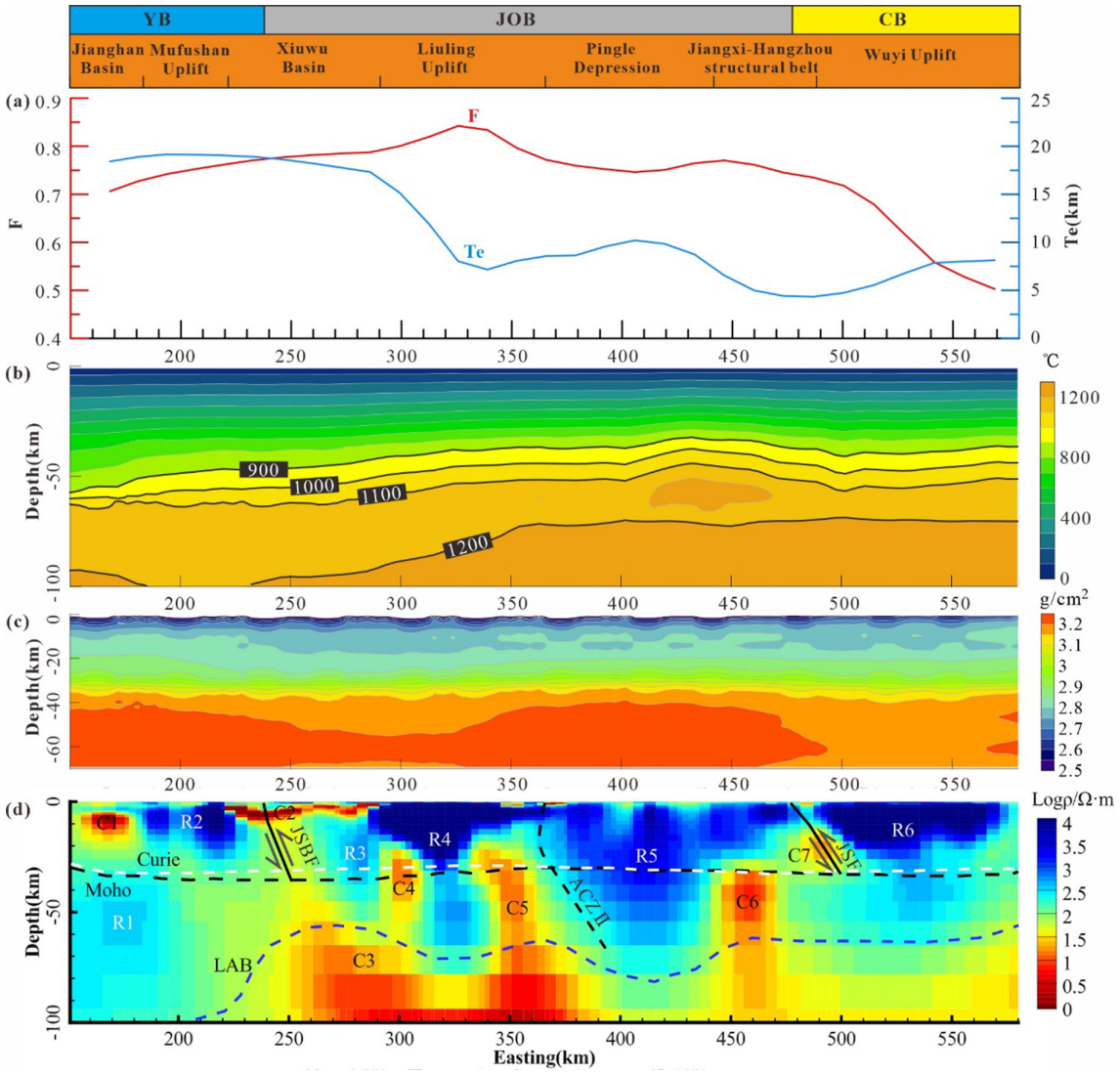

FIGURE 7: Electrical structure and comprehensive interpretation. (a) The load ratio and effective elastic thickness; (b) Thermal structure of lithosphere; (c) Lithospheric density; (d) Resistivity profile; Moho, Moho depth; LAB, Interface between lithosphere and asthenosphere; Curie, Curie depth [45, 46].

distribution morphology is in good agreement with the lithospheric low-velocity anomaly revealed by the 3-D shear wave velocity structure near the JSBF [48] (Figure 7). Therefore, JSBF, the NW boundary of the JOB, is inserted into the lower crust in the southeast direction of the deep part, reflecting the southeast deep subduction process of the Paleo-south China Ocean (Charvet, 2013; Yan et al., 2019) during the period of 970–860 Ma (Figure 8). Since the influence of fluid void pressure in the oceanic subduction zone usually causes the subducted ocean crust to carry a large amount of water into the crust and even the upper mantle [49], the in-shell high-conductivity C4 on the southeast side of JSBF is well related to the increase in the water content of the overlying crust caused by the subduction of the Paleo-south China crust, resulting in partial melting. The deep conductivity anomaly C3 may be an electrical reflection of the asthenosphere, which coincides with the higher geothermal flux value of 80–90 mW/m^2 in this region [46].

5.1.2 Jiangshan–Shaoxing Fault. At present, the academic understanding of the JSF zone as the south-east boundary of the JOB has basically become a consensus, but there is still a lot of controversy about whether and how the fault continues to extend to the west [5, 11, 38, 50, 51]. Through stratigraphic sequence analysis on the west side of the JOB, the researchers concluded that the south-east boundary of the JOB is the Shaoxing–Jiangshan–Pingxiang–Shuangpai line [38], as shown by JSF* in Figure 1. Through comprehensive geophysical data, other researchers believe that the deep part of the southeast boundary of the JOB may be spread along the Zhoushan–Shaoxing–Jinhua–Shangrao–Fuzhou–Ji'annan–Hezhou–Wuzhou–Beihai East line [5], which is consistent with the Phanerozoic boundary along the Jiangshao–Pingxiang–Qinfang line on

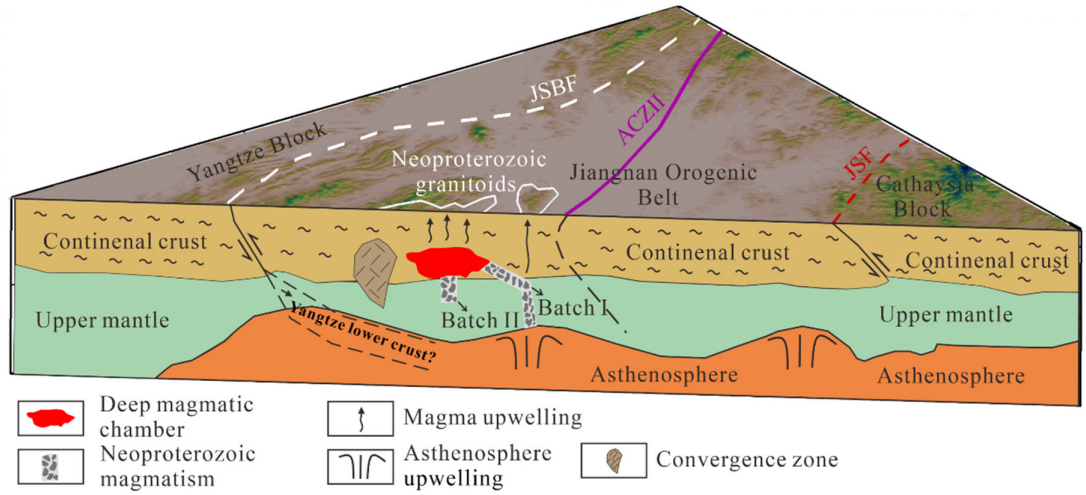

Figure 8: Schematic diagram of the contact relationship between the middle segment of the JOB and the Yangtze and Cathaysia blocks

the southeast side of the JOB revealed by previous studies [2], as shown by JSF in Figure 1. The high-conductivity anomaly C7 reflected in the 3-D electrical structure model in this paper has a good spatial map-ping relationship with JSF, which may reflect the westward extension of the JSF, which is similar to the situation revealed by predecessors based on the 2-D electrical structure of the geodetic electromagnetic profile of Jingdezhen–Wenzhou [27] and the 3-D electrical structure of geodetic electromagnetism in southeastern South China [12].

Although JSF marks the contact location between the JOB and the Cathaysia Block, its deep contact relationship and formation process are still controversial. Some researchers believe that the Cathaysia Block subducted below the JOB during the orogeny process [7, 52], but some scholars believe that the JOB subducted below the Cathaysia Block on the southeast side based on the volcanic arc assemblage found on both sides of the JOB [10]. There are also differences between onshore orogeny and magmatic activity or collision and extrusion [4, 53, 54]. The JSF revealed in this study has a southeastward dip feature in the deep, indicating that the JOB subducted the Cathaysia Block (Figure 8), which is consistent with the NW-SE compression in the Wuyi Yunkai area in the early Paleozoic, leading to the uplift of the Cathaysia Block [55]. In addition, the P-wave velocity structure revealed a high-speed anomaly extending downward from the Yangtze Block to the Cathaysia Block [56], which also confirms the deep extension of JSF reflected in the electrical structure of this paper. Since the SCC was affected by the Paleo-Pacific Plate subduction during the Late Mesozoic, the lithospheric mantle may have undergone a process of stretching and thinning [4]. Moreover, the satellite heavy magnetic data show that the region has a shallow inner depth, low effective elastic thickness, and high load ratio [46], which has a good correspondence with the high conductor C6 on the 3-D electrical structure model in this paper (Figure 7). Therefore, this conductivity anomaly may be related to asthenosphere upwelling caused by the Late Mesozoic lithospheric thinning (Figure 8). These tectonic–magmatic processes probably changed the Neoproterozoic structure, giving the JSF its current deep extension features.

5.2 Insights into Neoproterozoic Magmatic Processes. The genesis mechanism and tectonic background of Neoproterozoic granite in Jiuling area remain extremely disputed, despite extensive investigation yielding a number of positive discoveries [24, 39, 57]. The zircon U-Pb dating and Hf and O isotopic characteristics of Jiuling granite indicate that there were east-west differences in the granite source zone. The western source zone was melted by ancient crust, while the eastern source zone was melted by the juvenile arc crust and the granite here has a compositional evolution process from I-type to S-type [57]. In addition, the diagenetic age on the southeast side is earlier than that on the NW side, with a deeper magmatic origin depth and a higher degree of rock mass denudation [24, 25]. The analysis of the crystallization process of zircon and garnet from the Jiuling granite indicates that it is likely formed by the mixing of two batches of magma [39]. It can be seen that there is a basic consensus on the existence of two magma source zones of the Jiuling granite. From the obtained electrical structure model in this paper, the downward extension depth of the conductivity anomaly C5 on the southeast side of the Jiuling area is significantly deeper than that of the conductivity anomaly C4 on the west side, and there is a tendency to communicate with the mantle conductivity anomaly C3 (Figure 7), indicating that these two conductivity may have been formed by different geological processes. Therefore, we speculated that C4 and C5 may be electrical reflections of different source zones of the Jiuling granite. Due to the fact that C5 extends southeastward from the lower crust to the deep upper mantle, a large amount of crustal material may have been added in its later evolution, and lateral flow may have occurred towards the NW during the upward migration process (Figure 8). Previous studies have shown that soft collisions between Yangtze and Cathaysia Blocks along the Anhuinan–Jiuling–Xuefengshan–Sipu line during the 850–820 Ma period formed the ACZII [2], which may lead

to the formation of two different medium-acid magma by the bottom intrusion of water-bearing basalt magma in the island arc area of the continental margin [58–60]. Among them, the first stage magma is a water-rich residual magma generated by the separation and crystallization of basalt magma. The conductivity C5 extends to the deep part and communicates with the asthenosphere, it is likely to provide a favorable channel for the upwelling of the asthenosphere to form the source area of basalt magma. The second stage of magma is the shell-source magma produced by partial melting of the ancient crust after heating, which is consistent with the characteristics of the high-conductivity anomaly C4 near the lower crust on the NW side of the Jiuling area. It can be seen that the electrical structure obtained in this paper confirms the origin of different magma in the region. Based on our results, we proposed that the soft collision between the Yangtze and Cathaysia Blocks in the Jinning period II caused an asthenosphere upwelling, triggering first stage of magmatic activity and leading to the emplacement of the magma source zone on the southeast side of the Jiuling area. The magma continued to emplace upward during the extension stage after *t* collision, and mixed with a large amount of partially melted crustal material, forming the early granite on the southeast side of the Jiuling area. As the magma continued to rise and flow laterally towards the NW, partial melting occurred in the ancient lower crust of the area after heating, triggering the formation of the late granite on the NW side of the Jiuling area in the second stage of magmatic activity.

6. Conclusion

This study presents a stable and reliable lithospheric electrical structure model constructed by 3-D inversion of the MT data in the middle segment of the JOB. The main conclusions are as follows.

(1) The crustal electrical structure in the middle segment of the JOB is characterized by large-scale high resistivity and separated by several high-conductivity anomalies dipping southeast. The electrical structure of the upper mantle in this region is relatively complex, with significant differences in lateral resistivity distribution, and multiple high-conductivity and low-density anomalies at the crust-mantle scale.

(2) The JSBF forms the NW boundary of the middle segment of the JOB, and extends southeastward in the deep part; As the southeast boundary of the JOB, the deep extension of the JSF reflects the tectonic process of subduction of the JOB under the Cathaysia Block.

(3) The crustal high conductivity in the Jiuling area is considered to be an electrical reflection of the partial melting of the lower crust, possibly related to the southeastward subduction of the Paleo-south China Ocean during the 970–860 Ma period. The crust-mantle high conduction adjacent to the ACZII is likely related to the soft collision of the Yangtze and Catahysia Blocks that occurred along the Anhui–Jiuling–Xuefeng Mountain–Sipu line during Neoproterozoic. It is speculated that the asthenosphere upwelling caused by this collision may be the deep geodynamic mechanism of synchronous magmatic activity in the Jiuling area.

Data Availability

Data associated with this research are available and can be obtained by contacting the corresponding author.

Conflicts of Interest

The authors declare no conflict of interest.

Acknowledgments

We acknowledge all those who participated in the field data collection. We thank the authors of ModEM for providing the MT inversion code. We are grateful to the anonymous reviewers for their critical reviews and suggestions, which substantially improved the quality of the paper.
This paper is financially supported by the National Natural Science Foundation of China (U2344220, 42130811, 42304090, 41864004, 42274185, 42064008, 92062108), the Open Project of the Laboratory of Deep Earth Science and Exploration Technology of the Ministry of Natural Resources (Sino probe Lab 202214), and the Science and Technology Project of Jiangxi Province (20204BCJL23058, 20224BAB203046), the Open Fund of State Key Laboratory of Nuclear Resources and Environment (2022NRE18).

References

[1] Y. K. Li, J. W. Gao, J. Han, et al., "Geophysical evidence for thrusting of Crustal materials from Orogenic belts over both sides of the Yangtze block and its geological significance," *Science China Earth Sciences*, vol. 62, no. 5, pp. 812–831, 2019.

[2] G. W. Zhang, A. L. Guo, Y. J. Wang, et al., "Tectonics of South China continent and its implications," *Science China Earth Sciences*, vol. 56, no. 11, pp. 1804–1828, 2013.

[3] Y. Q. Zhang, Q. T. Lü, J. Y. Yan, et al., "Crustal structure of the middle segment of the Jiangnan Orogen and its implications on mineralization: revealed by teleseismic receiver functions along the Guangchang-Liuyang profile," *Acta Petrologica Sinica*, vol. 38, no. 2, pp. 559–572, 2022.

[4] L. S. Shu, "An analysis of principal features of tectonic evolution in South China block," *Geological Bulletin of China*, vol. 31, no. 7, pp. 1035–1053, 2012.

[5] J. Y. Yan, Q. T. Lü, Y. Q. Zhang, et al., "The deep boundaries of Jiangnan Orogenic belt and its constraints

on metallogenic: from the understanding of integrated geophysics," *Acta Petrologica Sinica*, vol. 38, no. 2, pp. 544–558, 2022.

[6] L. Z. Guo, Y. S. Shi, H. F. Lu, et al, "The pre-Devonian Tectonic patterns and evolution of South China," *Journal of Southeast Asian Earth Sciences*, vol. 3, nos. 1–4, pp. 87–93, 1989.

[7] J. H. Zhao, M. F. Zhou, D. P. Yan, et al, "Reappraisal of the ages of Neoproterozoic strata in South China: no connection with the Grenvillian Orogeny," *Geology*, vol. 39, no. 4, pp. 299–302, 2011.

[8] X. H. Li, W. X. Li, Z. X. Li, et al., "Amalgamation between the Yangtze and Cathaysia Blocks in South China: constraints from SHRIMP U–Pb zircon ages, geochemistry and Nd–HF isotopes of the Shuangxiwu volcanic rocks," *Precambrian Research*, vol. 174, nos. 1–2, pp. 117–128, 2009.

[9] Y. F. Zheng, R. X. Wu, Y. B. Wu, et al., "Rift melting of juvenile arc-derived crust: Geochemical evidence from Neoproterozoic volcanic and Granitic rocks in the Jiangnan Orogen, South China," *Precambrian Research*, vol. 163, nos. 3–4, pp. 351–383, 2008.

[10] G. C. Zhao, "Jiangnan Orogen in South China: developing from divergent double subduction," *Gondwana Research*, vol. 27, no. 3, pp. 1173–1180, 2015.

[11] X. L. Wang, J. C. Zhou, X. Chen, et al., "Formation and evolution of the Jiangnan Orogen," *Bulletin of Mineralogy, Petrology and Geochemistry*, vol. 36, no. 5, pp. 714–735, 2017.

[12] S. Xu, M. J. Unsworth, X. Y. Hu, et al., "Magnetotelluric evidence for asymmetric simple shear extension and Lithospheric thinning in South China," *Acta Geologica Sinica - English Edition*, vol. 93, no. S1, pp. 92–93, 2019.

[13] X. Mao, G. F. Ye, Y. X. Zhang, et al., "Electric structure of the Southern section of the Jiangnan Orogenic belt and its Tectonic implications," *Chinese Journal of Geophysics*, vol. 64, no. 11, pp. 4043–4059, 2021.

[14] J. Y. Wang, "New development of magnetotelluric sounding (MT) in China," *Chinese Journal of Geophysics*, no. S1, pp. 206–216, 1997.

[15] W. B. Wei, "New advance and prospect of magnetotelluric sounding (MT) in China," *Progress in Geophysics*, vol. 2, pp. 245–254, 2002.

[16] S. W. Dong, T. D. Li, X. H. Chen, et al, "Progress of deep exploration in mainland China: a review," *Chinese Journal of Geophysics*, vol. 55, no. 12, pp. 3884–3901, 2012.

[17] N. M. Meqbel, G. D. Egbert, P. E. Wannamaker, et al, "Deep electrical Resistivity structure of the Northwestern U.S. derived from 3-D inversion of Usarray Magnetotelluric data," *Earth and Planetary Science Letters*, vol. 402, pp. 290–304, 2014.

[18] J. Z. Deng, H. Chen, C. C. Yin, et al, "Three-dimensional electrical structures and significance for mineral exploration in the Jiujiang-Ruichang district," *Chinese Journal of Geophysics*, vol. 58, no. 12, pp. 4465–4477, 2015.

[19] H. Yu, J. Z. Deng, H. Chen, et al., "Three-dimensional magnetotelluric inversion under topographic relief based on the limited-memory quasi-Newton algorithm (L-BFGS)," *Chinese Journal of Geophysics*, vol. 62, no. 8, pp. 3175–3188, 2019.

[20] J. Deng, H. Yu, H. Chen, et al., "Ore-controlling structures of the Xiangshan volcanic basin, SE China: revealed from three-dimensional inversion of magnetotelluric data," *Ore Geology Reviews*, vol. 127, p. 103807, 2020.

[21] J. J. Sun, L. S. Shu, M. Santosh, et al, "Neoproterozoic Tectonic evolution of the Jiuling Terrane in the central Jiangnan Orogenic belt (South China): constraints from Magmatic suites," *Precambrian Research*, vol. 302, pp. 279–297, 2017.

[22] Z. H. Zhang, D. Zhang, X. L. He, et al, "Biotite granodiorite age of Jiuling complex in Jiangxi province and its limitation on the collision and splicing time of the Yangtze and Cathay plates," *Zgdz*, vol. 48, no. 5, pp. 1562–1579, 2021.

[23] J. H. Liu, F. Yong, Z. D. Liu, et al., "Crustal structure characteristics of the middle part of Jiangnan Orogenic belt: insights from random medium correlation length analysis of Wuning–Ji'an deep seismic reflection profile," *Acta Geoscientica Sinica*, 1–16, 2022.

[24] Z. Duan, G. F. Xing, S. B. Liao, et al, "Compositional difference from the sources of Jiuling Neoproterozoic granite complex in Eastern segment of the Jiangnan Orogen: constraints from geochemistry and HF Isotope of Zircons," *Acta Petrologica Sinica*, vol. 33, no. 11, pp. 3610–3634, 2017.

[25] Z. Duan, S. B. Liao, P. L. Chu, et al., "Zircon U-Pb ages of the Neoproterozoic Jiuling complex granitoid in the eastern segment of the Jiangnan Orogen and its tectonic significance," *Geology in China*, vol. 46, no. 3, pp. 493–516, 2019.

[26] C. X. Chen, J. Y. Yan, W. Q. Liu, et al., "Differences in crustal structure and composition in Wuling–middle part of Jiangnan Orogenic belt: based on geochemical and geophysical anomalies," *Acta Geoscientica Sinica*, 1–17, 2022.

[27] S. Han, G. X. Liu, and J. T. Han, "Deep electrical structure of Jingdezhen-Wenzhou magnetotelluric profile," *Chinese Journal of Geology*, vol. 51, no. 1, pp. 86–98, 2016.

[28] K. Zhang, Q. T. Lü, J. Zhao, et al., "Magnetotelluric evidence for the multi-microcontinental composition of eastern South China and its tectonic evolution," *Scientific Reports*, vol. 10, no. 1, 2020.

[29] J. E. Dong, G. F. Ye, W. B. Wei, et al., "Structural characteristics, mineralization and dynamic mechanism of the northeast South China block: understanding from magnetotelluric data," *Geological Review*, vol. 68, no. 3, pp. 921–937, 2022.

[30] G. D. Egbert, "Robust multiple-station magnetotelluric data processing," *Geophysical Journal International*, vol. 130, no. 2, pp. 475–496, 1997.

[31] T. G. Caldwell, H. M. Bibby, and C. Brown, "The magnetotelluric phase tensor," *Geophysical Journal International*, vol. 158, no. 2, pp. 457–469, 2004.

[32] J. R. Booker, "The magnetotelluric phase tensor: a critical review," *Surveys in Geophysics*, vol. 35, no. 1, pp. 7–40, 2014.

[33] A. Kelbert, N. Meqbel, G. D. Egbert, et al., "Modem: a modular system for inversion of electromagnetic geophysical data," *Computers & Geosciences*, vol. 66, pp. 40–53, 2014.

[34] A. W. Liu, D. Q. Tang, L. B. Guo, et al., "Differential segmental activities of Qianbei fault zone in Jianghan basin and its evolution," *Oil Geophysical Prospecting*, vol. 57, no. 4, pp. 937–949, 2022.

[35] H. C. Shi, X. B. Shi, X. Q. Yang, et al., "The Exhumation process of Mufushan granite in Jiangnan uplift since Cenozoic: evidence from low-temperature Thermochronology," *Chinese Journal of Geophysics*, vol. 56, no. 3, pp. 273–286, 2013.

[36] C. H. Wen, X. Y. Luo, J. F. Chen, et al., "Relationship between Yanshanian Magmatic activity and rare metal mineralization in Mufushan area of Northeast Hunan," *Geological Survey of China*, vol. 6, pp. 19–28, 2019.

[37] W. W. Liu, *"The Cambrian-Silurian Black Shale Reservoir Characteristics and Reservoir-Forming Condition in Xiuwu Basin,"* Chengdu University of Technology, Sichuan Province, China, 2015.

[38] J. L. Yao, L. S. Shu, M. Santosh, et al., "Neoproterozoic arc-related Mafic–Ultramafic rocks and Syn-collision granite from the Western segment of the Jiangnan Orogen, South China: constraints on the Neoproterozoic assembly of the Yangtze and Cathaysia blocks," *Precambrian Research*, vol. 243, pp. 39–62, 2014.

[39] W. Rong, *"A Geochemical Study of Neoproterozoic Granites from the Jiuling Range,"*, University of Science and Technology of China, Anhui province, China, 2018.

[40] N. Q. Liu, R. J. Qin, M. S. Chen, et al., "Study of transform like fault and rock-and ore-controlling role in the northern Jiangxi province," *Acta Geologica Sinica*, vol. 96, no. 6, pp. 1957–1971, 2022.

[41] H. Z. Wang and X. X. Mo, "The geological structure of China," *Geology in China*, vol. 1996, no. 8, pp. 4–9, 1996

[42] X. Q. Yu, G. G. Wu, L. S. Shu, et al, "The Cretaceous Tectonism of the gan-hang Tectonic belt, southeastern China," *Earth Science Frontiers*, vol. 2006, no. 3, pp. 31–43, 2006.

[43] S. Y. Yang, "Petrogenesis and Geodynamic Setting of Magmatic Rocks from Uranium-Bearing Volcanic Basins, Gan-Hang Belt," Nanjing University, Jiangsu Province, China, 2013.

[44] Y. F. Deng, S. L. Li, W. M. Fan, et al., "Crustal structure beneath South China revealed by deep seismic soundings and its dynamics implications," *Chinese Journal of Geophysics*, vol. 54, no. 10, pp. 2560–2574, 2011.

[45] Y. Zhang, D. Shi, Q. Lü, et al., "The crustal thickness and composition in the eastern South China block constrained by receiver functions: implications for the geological setting and metallogenesis," *Ore Geology Reviews*, vol. 130, no. 1, p. 103988, 2021.

[46] F. Luo, J. Y. Yan, C. Zhang, et al., "The effective elastic thickness of lithosphere and its tectonic implications in the South China block," *Acta Geoscientica Sinica*, 1–14, 2022.

[47] L. S. Shu, J. Q. Wang, and J. L. Yao, "Tectonic evolution of the eastern Jiangnan region, South China: new findings and implications on the assembly of the Rodinia supercontinent," *Precambrian Research*, vol. 322, pp. 42–65, 2019.

[48] S. Luo, H. Yao, Q. Li, et al., "High-resolution 3D crustal S-wave velocity structure of the middle-lower Yangtze river metallogenic belt and implications for its deep geodynamic setting," *Science China Earth Sciences*, vol. 62, no. 9, pp. 1361–1378, 2019.

[49] S. M. Peacock, N. I. Christensen, M. G. Bostock, et al., "High pore pressures and porosity at 35 km depth in the Cascadia Subduction zone," *Geology*, vol. 39, no. 5, pp. 471–474, 2011.

[50] L. S. Shu, X. M. Zhou, P. Deng, et al., "Mesozoic tectonic evolution of the southeast China block: new insights from basin analysis," *Journal of Asian Earth Sciences*, vol. 34, no. 3, pp. 376–391, 2009.

[51] L. S. Shu, J. L. Yao, B. Wang, et al., "Neoproterozoic plate tectonic process and phanerozoic geodynamic evolution of the South China block," *Earth-Science Reviews*, vol. 216, p. 103596, 2021.

[52] X. H. Li, W. X. Li, and Z. X. Li, "Re-discuss the genetic type and tectonic significance of the early Yanshanian granites in Nanling," *Chinese Science Bulletin*, vol. 52, no. 9, pp. 981–991, 2007.

[53] Z. X. Li and X. H. Li, "Formation of the 1300-km-wide intracontinental orogen and postorogenic magmatic province in Mesozoic South China: a flat-slab subduction model," *Geology*, vol. 35, no. 2, pp. 179–182, 2007.

[54] J. H. Yang, "Detrital record of collision and Exhumation processes of Orogen," China University of Geosciences, Hubei Province, China, 2012.

[55] M. Faure, L. S. Shu, B. Wang, et al., "Intracontinental Subduction: a possible mechanism for the early Palaeozoic Orogen of SE China," *Terra Nova*, vol. 21, no. 5, pp. 360–368, 2009.

[56] Z. C. Huang, L. S. Wang, D. P. Zhao, et al., "Upper mantle structure and dynamics beneath Southeast China," *Physics of the Earth and Planetary Interiors*, vol. 182, nos. 3–4, pp. 161–169, 2010.

[57] X. L. Wang, J. C. Zhou, Y. S. Wan, et al., "Magmatic evolution and crustal recycling for Neoproterozoic strongly peraluminous granitoids from southern China: HF and O isotopes in zircon," *Earth and Planetary Science Letters*, vol. 366, pp. 71–82, 2013.

[58] C. Annen, J. D. Blundy, and R. S. J. Sparks, "The genesis of intermediate and silicic magmas in deep crustal hot zones," *Journal of Petrology*, vol. 47, no. 3, pp. 505–539, 2006.

[59] J. M. S. Solano, M. D. Jackson, R. S. J. Sparks, et al., "Melt segregation in deep crustal hot zones: a mechanism for chemical differentiation, crustal assimilation and the formation of evolved magmas," *Journal of Petrology*, vol. 53, no. 10, pp. 1999–2026, 2012.

[60] X. L. Wang, "Formation and evolution of the Jiangnan Orogen," *Bulletin of Mineralogy, Petrology and Geochemistry*, vol. 33, pp. 1445–1458, 2017.